Carbon Nanotube Templated Manufacturing of Hierarchically Structured Fluid Filters

Andrew Davis

A senior thesis submitted to the faculty of
Brigham Young University
in partial fulfillment of the requirements for the degree of

Bachelor of Science

Robert Davis and Richard Vanfleet, Advisors

Department of Physics and Astronomy

Brigham Young University

April 2016

Copyright © 2016 Andrew Davis

All Rights Reserved

ABSTRACT

Carbon Nanotube Templated Manufacturing of Hierarchically Structured Fluid Filters

Andrew Davis
Department of Physics and Astronomy, BYU
Bachelor of Science

Here we demonstrate the fabrication of two types of fluid filters developed using carbon-nanotube-templated microfabrication (CNT-M). The first of these are high strength microsieves for both liquid and gas filtration. The sieves were fabricated by growing patterned forests of vertically aligned carbon nanotubes followed by an infiltration of the forest with nanocrystalline carbon. The process is compatible with the fabrication of sieves with pore sizes from below one micron up to tens of microns. Straight, vertical channels result in low flow resistance and the high strength carbon material is compatible with high pressure filtering. Initial filtration testing on sample sieves with 5 micron pores showed greater than 99.5% removal efficiencies of 6 micron particles. The second filter type also uses an adaptation of CNT-M to make high throughput filters by hierachically patterning the structure to achieve ultrahigh surface areas. These filters have pores on the order of 50-100 nm and therefore are compatible with bacterial filtration. Preliminary flow testing has shown flow rates of over 180 times greater than standard Millipore mixed cellulose ester sterilizing disk filters.

Keywords: Microsieve, nanosieve, membrane, filtration, absolute filter, vertically aligned carbon nanotubes, chemical vapor infiltration, CNT templated microfabrication, particle enrichment, precision pores, bacterial filtration, high throughput filtration, sterilization

Contents

Table of Contents iii

1 Introduction 1
- 1.1 Microsieves . . . 1
- 1.2 Sterilization Filtration . . . 2
- 1.3 Carbon Nanotube Templated Microfabrication . . . 2
- 1.4 Filter Characterization . . . 3
- 1.5 Overview . . . 3

2 Materials and Methods 4
- 2.1 Filter Fabrication . . . 4
  - 2.1.1 Substrate Preparation . . . 6
  - 2.1.2 Photolithography . . . 6
  - 2.1.3 Iron Deposition and Patterning . . . 7
  - 2.1.4 CNT Growth and Infiltration . . . 7
  - 2.1.5 Removing the Floor Layer . . . 8
- 2.2 Ultrahigh Surface Area Filter Fabrication . . . 8
- 2.3 Pressure vs Flow Rate Testing . . . 12
  - 2.3.1 Microsive Flow Testing . . . 13
  - 2.3.2 Ultrahigh Surface Area Filter Flow Testing . . . 13
- 2.4 Efficiency Testing . . . 13
  - 2.4.1 Microsieve Efficiency Testing . . . 13
  - 2.4.2 Ultrahigh Surface Area Filter Efficiency Testing . . . 14

3 Results and Conclusions 15
- 3.1 Filter Physical Characterization . . . 15
  - 3.1.1 Microsieve Physical Characterization . . . 15
  - 3.1.2 Ultrahigh Surface Area Filter Characterization . . . 17
- 3.2 Pressure vs Flow Rate Results . . . 18
  - 3.2.1 Microsive Flow Rate Results . . . 18
  - 3.2.2 Ultrahigh Surface Area Filter Flow Results . . . 20
- 3.3 Microsieve Efficiency Results . . . 21

3.4 Conclusion 23

Bibliography **24**

Index **26**

Chapter 1

Introduction

1.1 Microsieves

Microsieves are size exclusion filters with precise arrays of straight pores of uniform size and shape. Precisely defined arrays of pores allows for high pore densities while maintaining membrane strength. Straight, uniform pores provide lower flow resistance. High pore densities and low pore flow resistance make microsieves desirable for their low pressure drop and therefore high through-membrane flow rate over other microfiltration media. [1] Microsieves are used for many filtration processes including particle separation and analysis, blood filtering, water purification, membrane emulsification, and purification of materials used in semiconductor electronics. [2]

Microsieves have previously been fabricated from silicon nitride, silicon, polymers, and metals. [3] [4] [5] Silicon nitride microsieves are chemically inert and can withstand high temperatures. These nitride membranes are produced by low pressure chemical vapor deposition of silicon nitride thin films which are then patterned with reactive ion etching. Consequently they have only been produced at very low aspect ratios and thicknesses under approximately 2 micron. Because silicon nitride is very brittle, at these thicknesses the membranes are extremely fragile. Silicon

microsieves have also been fabricated, but share the same difficulties of silicon nitride membranes. Polymer microsieves have been fabricated using phase separation micromolding, photolithography, and hot molding. Although polymer membranes can be fabricated at variable thicknesses and pore diameters, they are less chemically inert than inorganic membranes and are not compatible with high temperature filtration. Metal microsieves are generally fabricated using electroplating on molds and are difficult to release at thicknesses over a few hundred nanometers for pore sizes in the sub-micron range. Though metal microsieves are chemically inert and unaffected by high temperature, they also are extremely fragile because they are so thin.

The most commonly used filters with uniform pore sizes are track etch membranes. Though track etch membranes are not true microsieves because they have a random placement of pores, they have relatively uniform pore sizes.

1.2 Sterilization Filtration

One of the best known uses of filters is for bacterial removal. Bacterial removal requires filters with pore sizes of under 0.22 microns. Because of the small pores size required, sterilizing filters often struggle to achieve high flow rates. In order to overcome this challenge large filter areas are often used. In order to achieve large filter areas in relatively small form factors sterilizing filters are generally pleated with tighter pleating allowing for higher surface areas in the same form factor. As an alternative to pleating, some filter materials are made into a series of hollow fibers that serve the same purpose of increasing the surface area to volume ratio.

1.3 Carbon Nanotube Templated Microfabrication

Carbon Nanotube Templated Microfabrication is a additive fabrication technique that was developed at Brigham Young University. [6] The CNT-M process was developed to fabricate 3-

dimensional structures by growing patterned forests of vertically aligned carbon nanotubes (VACNT) followed by an infiltration of the forest with nano-crystalline graphite or other infiltration materials. CNT-M can be used to fabricate high aspect ratio structures using a wide range of ceramic and metal infiltration materials and with feature sizes down to ca. 1 micron and heights from 10 microns to 1 mm. [7]

1.4 Filter Characterization

Some of the most important metrics by which filters are characterized are pore size distribution, particle removal efficiencies, flow rate, and burst pressure. One of the most comprehensive methods of measuring pore size and particle removal efficiencies is by using test particles of known sizes. Concentrations of different size particles are measured before and after filtration. This gives removal efficiencies for different particle sizes. Flow rate and burst pressure can be measured by driving clean water through the filter at set flow rates and then measuring the differential pressure. The burst pressure can be measured by slowly increasing the flow rate until the filter bursts while measuring the pressure. A sudden drop in pressure implies filter failure.

1.5 Overview

In Chapter 2 we explain the fabrication techniques used for both the microsieves and the ultrahigh surface area (UHSA) filter geometries. We also describe the filter characterization methods used. In Chapter 3 we discus the characterization results for each filter type.

Chapter 2

Materials and Methods

In Section 2.1 we discus the microsieve fabrication process in detail. Section 2.2 describes the adaptations used for fabricating the UHSA filters. In sections 2.3 and 2.4 we describe the methods we used to characterize the filters.

2.1 Filter Fabrication

Using an adaptation of CNT-M, 1 cm diameter filters with 5 micron x 10 micron diamond shaped pores are fabricated. (Figure 2.1 has a diagram of the process which will be explained in the rest of this section). The first half of this process (alumina deposition and photolithography) is done in a class 100 cleanroom in order to prevent airborne particulates from landing on the sample surface and interfering with the patterning. Even after the sample is removed from the cleanroom, care is taken to keep the sample clean. It is only removed from the closed sample container when necessary and only briefly. Any time the sample is exposed to non-cleanroom air, particulates are landing on the surface. The sample is only touched on the edges by tweezers or gloved hands. The surface should never be touched. If particulates are visible on the sample surface, some can be removed using a clean nitrogen blow gun.

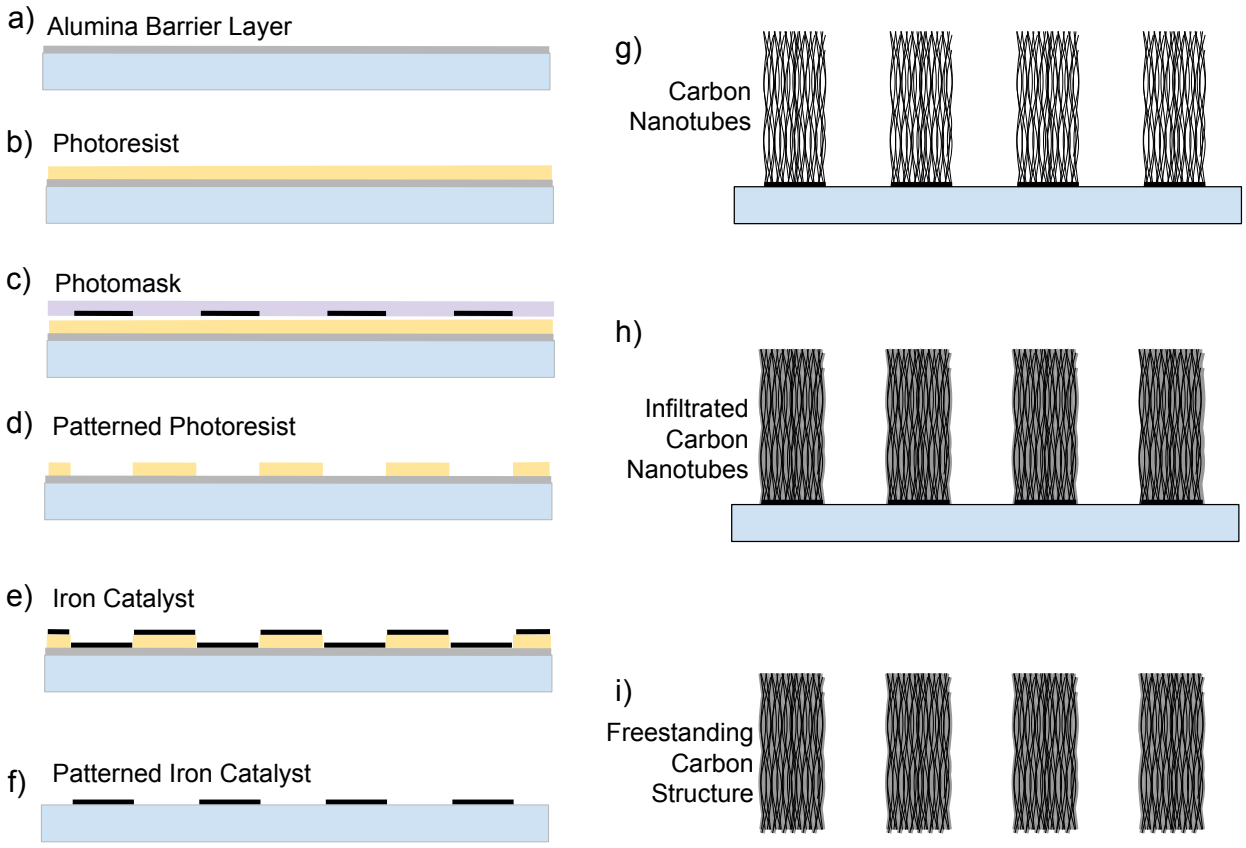


Figure 2.1 Carbon Nanotube Templated Microfabrication. a) An alumina barrier layer is evaporated onto a silicon wafer substrate. b) Photoresist is spun on top of the alumina. c) A photomask is placed on the photoresist. UV light is shown through the photomask, exposing the photoresist wherever there is no chrome. d) Photoresist not exposed to UV light is dissolved using the photoresist developer, leaving a patterned photoresist layer. e) An iron catalyst layer is evaporated onto the patterned photoresist. f) The remaining photoresist is dissolved leaving behind a patterned iron layer. g) Carbon nanotubes (CNT) are grown from the iron catalyst by placing the sample in a tube furnace and flowing hydrogen and ethylene gas over over it at 750 °C. h) The temperature on the furnace is then ramped to 900 °C which causes nanocrystalline carbon to deposit onto the surface of the nanotubes. This infiltration of the forest locks the nanotubes together and forms a mostly solid carbon structure. i) The final carbon structure is then removed from the silicon substrate.

2.1.1 Substrate Preparation

Fabrication is done on a 4 inch diameter silicon wafer substrate. A 30 nm barrier layer of alumina is deposited onto a silicon wafer using a Denton Vacuum E-beam Evaporator. See Figure 2.1.a. This layer prevents a subsequent iron layer from diffusing into the silicon when the sample is heated and provides an alumina layer for surface diffusion.

2.1.2 Photolithography

The filter pattern is made using a process called photolithography. Photolithography is a process that is commonly used in the semiconductor industry to pattern structures with micron scale resolution. To begin this process, AZ nLOF 2020 (a photoresist—a polymer that crosslinks when exposed to UV light) is spun over the alumina at 2750 rpm for 60 s. The photoresist is then soft-baked on a hotplate at 110 °C leaving approximately 2 microns of photoresist. See Figure 2.1.b. A photomask—a glass plate with patterned chrome on one side—was prepared with a chrome array of 5 micron x 10 micron diamonds separated by 3 micron spaces. The photomask is placed on top of the photoresist in hard contact using a Karl Suss MA 150 CC Mask Aligner. See Figure 2.1.c. The aligner then exposed the photoresist to UV light through the mask for 7 sec (a 70 mJ exposure). This starts crosslinking the photoresist in areas where there is no chrome on the photomask. The wafer is then placed on a hotplate at 110 °C to complete the polymer crosslinking process in areas where the photoresist was exposed to UV light. The photoresist is then developed in a AZ300MIF bath for 60 s. This dissolves the unexposed areas of the photoresist. See Figure 2.1.d. At this point the wafer is checked under a microscope. The diamond pattern should be clearly visible and clean (See Figure 2.2). A more detailed explication of the photolithography process can be found on the BYU cleanroom website at cleanroom.byu.edu.



Figure 2.2 Diamond pattern in photoresist

2.1.3 Iron Deposition and Patterning

Carbon-nanotubes grow from an iron catalyst layer. For the CNT-M process, a 4-7 nm thick iron film is deposited on top of the photoresist using thermal evaporation. See Figure 2.1.e. The remaining photoresist is lifted off by placing in a bath of Microposit 1165 or NMP. The bath is placed in the sonicator until no photoresist residue is visible. This usually takes about 20 min. After removing the sample from the bath it is checked under the microscope for any photoresist residue that wasn't visible to the eye. If there is remaining residue, the wafer is returned to the bath and sonicated for additional time (sometimes this can take a few hours). Removing the photoresist also removes any iron that was on top of the photoresist, leaving a grid of 3 micron wide patterned iron catalyst lines (the negative of the photoresist diamonds). See Figure 2.1.f.

2.1.4 CNT Growth and Infiltration

The nanotubes are grown from the patterned iron grid and then infiltrated. This is done using the following chemical vapor disposition (CVD) processes. The samples are cut into pieces about 1 cm square and then placed in a 1 inch quartz tube furnace (Lindberg Blue M EW-33850). The furnace is then heated to 750 °C while 375 sccm (standard cubic centimeter per minute) of H_2 is flowed through the tube. Heating the sample in H_2 allows the catalyst, which has oxidized by this point, to reduce and to form iron nanoparticles on the surface of the alumina. When the temperature reached 750 °C, the CNT forest growth is started by flowing 400 sccm of C_2H_4 and 375 sccm of

H_2 simultaneously. Growth time is 6 min for a target CNT height of 150 micron. See Figure 2.1.g. At the end of 6 min the H_2 and C_2H_4 is replaced by 400 sccm of Ar and the furnace is ramped to 900 °C. When 900 °C is reached, the forest is infiltrated with carbon by flowing 200 sccm of Ar and 190 sccm of C_2H_4 for 30 min. See Figure 2.1.h.The C_2H_4 is then turned off, and the sample is cooled under argon flow. When the furnace temperature is less than 700 °C the tube is removed from the furnace to speed cooling. To keep the nanotubes from burning, Ar flow is maintained until the tube temperature was below 200 °C. During cooling, the infiltrated, patterned forest self-released from the silicon substrate because of internal stress. If the sample does not self release, it can be released by soaking in KOH until it releases. (Infiltration using other materials are also possible. For more information about nickel infiltration see [8]. For silicon infiltration see [7]. For more details about the CNT growth procedure see [6]).

2.1.5 Removing the Floor Layer

The infiltration process results in a thin carbon floor layer which is removed by O_2 reactive ion etching (RIE). RIE is done on the bottom (side that was in contact with the silicon wafer) of the filter structure in an Anelva DEM-451 at 100 mTorr and 250 W with an O_2 flow rate of 100 sccm until floor layer was removed (the floor layer side of the sample becomes black and non-reflective. About 15 min in 5 minute increments).

2.2 Ultrahigh Surface Area Filter Fabrication

An adaptation of the CNT-M filter fabrication process was designed to make filters with ultrahigh surface area. This adaptation follows that shown in Figure 2.1 steps a–g, but the final steps are adapted to only partially infiltrate the CNT forest (See Figure 2.4.c). This allows for structures with has porous sidewalls (see Figure 2.3). These sidewalls are then used as the filter membrane.

In order to force the liquid through the forest sidewalls every other larger pore is plugged so that the liquid goes in one pore, through the sidewall, and out the next pore over. See Figure 2.4.d and Figure 2.5.

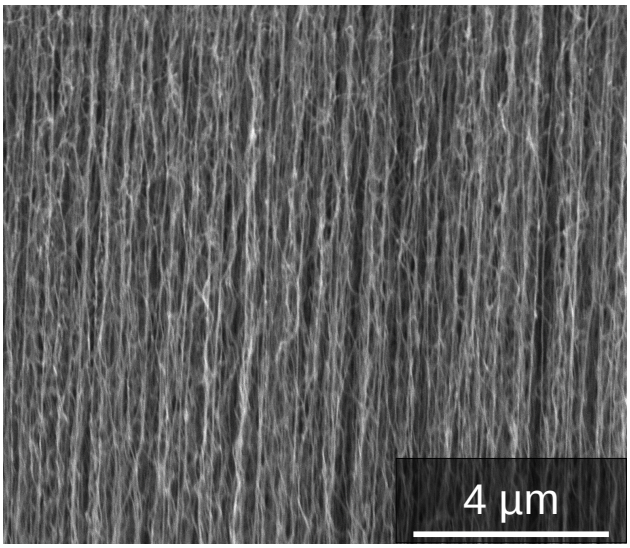


Figure 2.3 Porous sidewall of a partially infiltrated CNT forest

In order to test if filtering through the CNT forest sidewalls was feasable we developed a proof of concept UHSA design. It was patterned using a photomask with the design shown in Figure 2.6. Four variations of this design were on the mask. The large nine-square pattern was the same, but different sidewall thicknesses were used: 5 micron, 10 micron, 20 micron, 40 micron. Samples were grown for each pattern using the same process as for the mircosieves with 20 min CNT growth steps and infiltration times of 2 and 3 minutes. Because partial infiltration leaves less internal stress in the CNT structure, these samples did not self release and were left on the silicon wafer for the next processing steps.

Square polycarbonate pieces (1 cm x 1 cm) were made to cap the top and bottom of the filter. The top polycarbonate piece had nine holes drilled in it so that they could be positioned over the center of each square (See Figure 2.7 and the white squares in Figure 2.6). The top piece of polycarbonate was attached by heating the nanotube sample and slightly melting the polycarbonate to

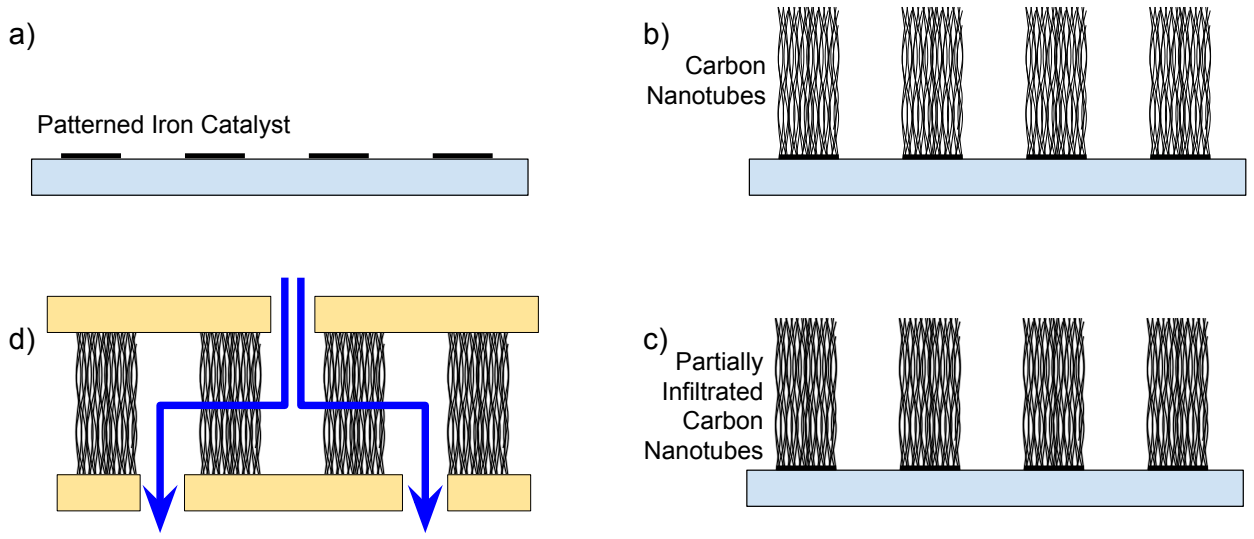


Figure 2.4 Ultrahigh Surface Area Process. The process is the same as for the standard CNT-M filters until the infiltration step. c) The carbon nanotubes are only partially infiltrated leaving a robust but porous structure. d) The structure is then released and every other pore is blocked so that fluid is forced through the forest's interstitial space.

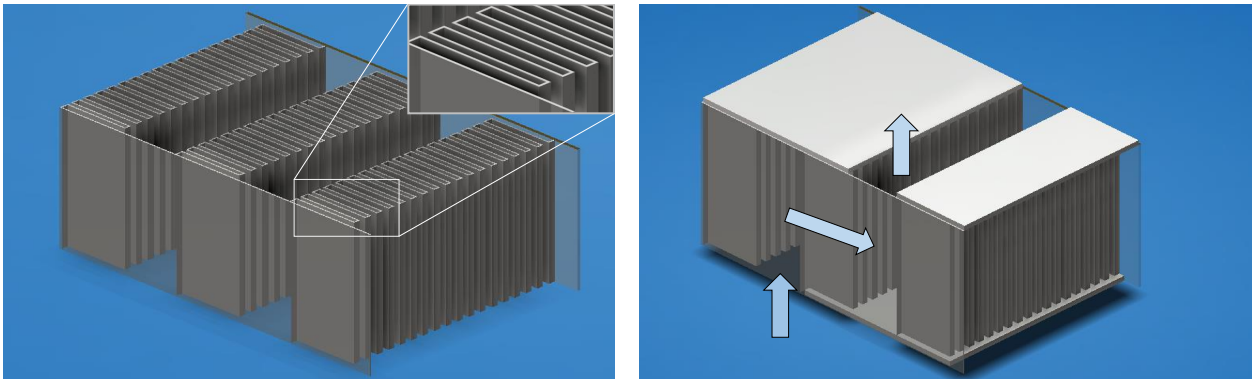


Figure 2.5 Theoretical Prototype of Ultrahigh Surface Area Geometry

seal it on the top. This was done by placing the samples on a cool hot-plate with the holes of the top polycarbonate piece alligned by centering them over the center of the nanotube forest squares. The hotplate was then set to 235 °C. When some areas of the polycarbonate piece started to attach to the CNT's (small areas of the CNT supports around the edges would go transparent/black, showing that the gap between the polycarbonate and the CNT had closed), a small flat piece of metal was placed on top of the polycarbonate and pressed down on the sample (about 3 pounds). When

the weight was pulled up, the whole CNT area had attached and gone black. The hotplate was then turned off and the sample was left there until the hotplate had cooled and the polycarbonate had fully hardened. As the sample cooled, the silicon wafer on the back popped off (most likely because the polycarbonate shrunk slightly as it cooled). The bottom polycarbonate piece was then attached on the other side of the filter using Conap Easypoxy. The epoxy was applied to one side of the bottom piece of polycarbonate and then all but a thin layer of epoxy was scraped off. The CNT filter was placed down on the epoxy and the epoxy was cured by placing the sample on a hotplate at 60 °C as detailed in the epoxy procedure.

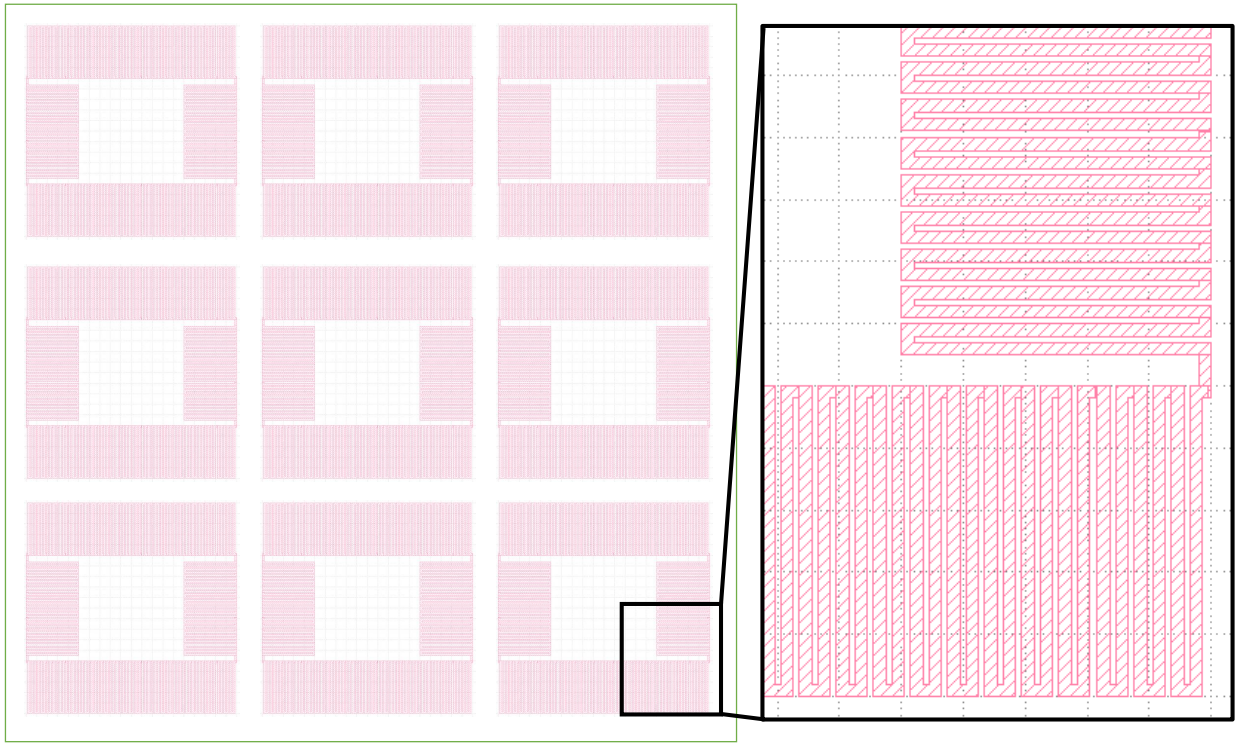


Figure 2.6 Ultrahigh Surface Area Proof Of Concept Design. This is the mask pattern used with the pink areas where the CNT's end up. Square polycarbonate caps were placed on the top and bottom of the forest. The top cap had holes that lined up with each of the white squares. The bottom cap was a solid square. When water was flowed through the holes in the top cap, it was forced out of through the nanotube forest sidewalls and out the side of the polycarbonate sandwich

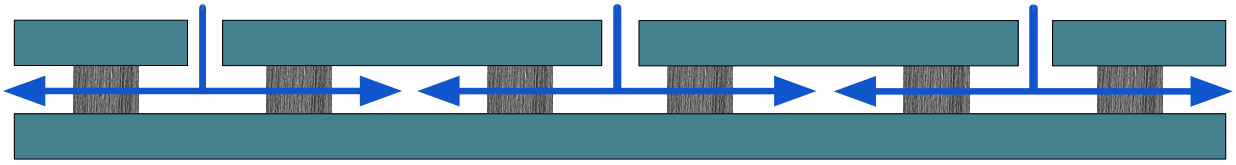


Figure 2.7 Ultrahigh Surface Area Proof Of Concept Design sideview. The top and bottom peices of the sandwich are polycarbonate. The middle layer is the partially infiltrated CNT forest. Water flow is shown by arrows.

2.3 Pressure vs Flow Rate Testing

The flow rate was tested by flowing deionized water through the filters using a syringe pump that allowed us to set the flow rate. The trans-filter pressure was measured at different flow rates using a differential pressure transducer. (See Figure 2.8)

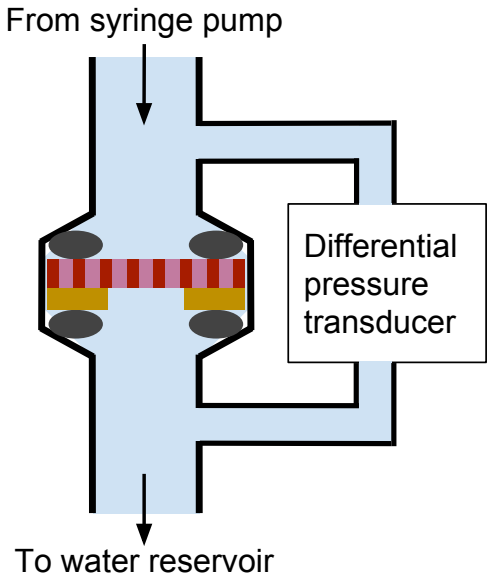


Figure 2.8 Flow Rate Testing Setup for Microsieves

2.3.1 Microsive Flow Testing

The flow rate for the microsieves was measured by setting the flow rate at 5 mL/min and the pressure was measured. In order to make sure that the filter stays clean and that the syringe doesn't run out of water, the flow was reversed at the same flow rate for the same time before moving on to the next flow rate. The flow rate was then increased by 5 mL/min and again the pressure was measured. This was repeated until the flow rate reached 105 mL/min. This entire cycle was run ten times on the same filter to check for degradation in filter performance.

2.3.2 Ultrahigh Surface Area Filter Flow Testing

The Flow rate for the UHSA filters were measured by super-gluing a coupling to the top polycarbonate piece so that water could be forced down through the nine squares and out through the sides of the polycarbonate sandwich. The same flow rate test setup was used as before, but, because the back coupling could not be attached, water was only forced through in the forward direction, and the differential pressure was measured using the room pressure as the downstream side.

2.4 Efficiency Testing

2.4.1 Microsieve Efficiency Testing

The microsieves particle removal efficiency was tested by taking solutions of fluorescent polystyrene particles of known sizes, 2 micron and 6 micron, and flowing them through the filter. Because the pore size is 5 microns we expect the 6 micron particles to be captured and the 2 micron particles to pass through the filter. The test was performed by gluing a completed filter sample to the end of a small glass tube. The fluorescence of a 1 mL solution of 6 micron fluorescent particles in suspension was measured. This solution was then pulled through the sample with a vacuum.

See Figure 2.9. The post-solution was then collected and the fluorescence was again measured and compared to the pre-filtration measurements. This same procedure was then repeated with 2 micron beads.

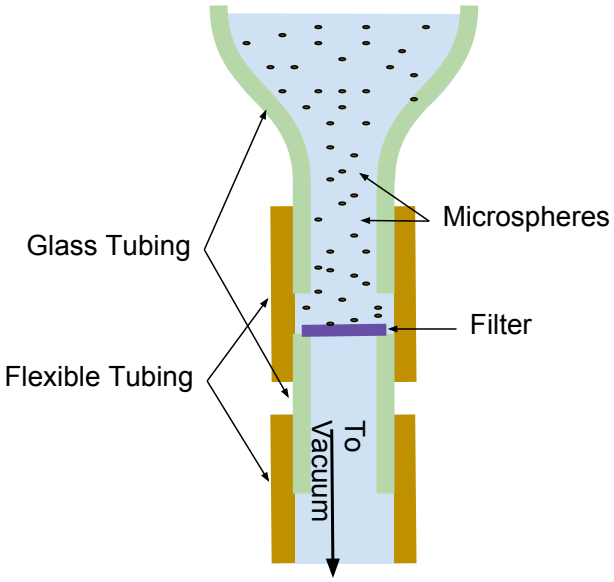


Figure 2.9 Efficiency Testing Setup

2.4.2 Ultrahigh Surface Area Filter Efficiency Testing

Efficiency testing was also attempted on the UHSA sieves by flowing bacteria through the filter using a hand syringe and then culturing the bacteria on the other side. Our proof of concept design had weak spots on each of the nine squares where each side of the square met. This area is shown in the close-up in Figure 2.6. When flowing the bacteria through the filter with the hand syringe the filters blew out at this point. Because the syringe pump used in flow testing was more controlled we don't think that the filters blew out during flow rate testing, but more data will need to be taken to confirm our flow rate data.

Chapter 3

Results and Conclusions

In this chapter we share the general physical characterization results and flow rate data for both types of filters, and share the particle removal efficiency results for the microsieves.

3.1 Filter Physical Characterization

3.1.1 Microsieve Physical Characterization

The CNT-M carbon process for microsieve fabrication results in a high fidelity structure that is substantially solid. Figure 3.1 shows Scanning Electron Microscope (SEM) images of a CNT-M filter structure grown from mask to produce 5 micron x 10 micron diamond pores. In Figure 3.1a the diamond pattern is visible on the top of the structure and the vertical lines are a cross sectional view where the filter was broken. Figure 3.1b is a higher magnification view of the top. These images show that the lithographic diamond pattern is faithfully reproduced in the final three dimensional structure. The cross section shows that the pores are straight and uniform vertically. Figure 3.1c shows that the surface roughness is well below one micron. Figure 3.1d is a high magnification image of a filter that was broken to show the infiltrated forest interior. The infiltration yielded a

substantially solid structure containing some nanoscale pockets or voids. Since the break tended to follow the pockets, it was not planar so the void volume fraction cannot be extracted from the image.

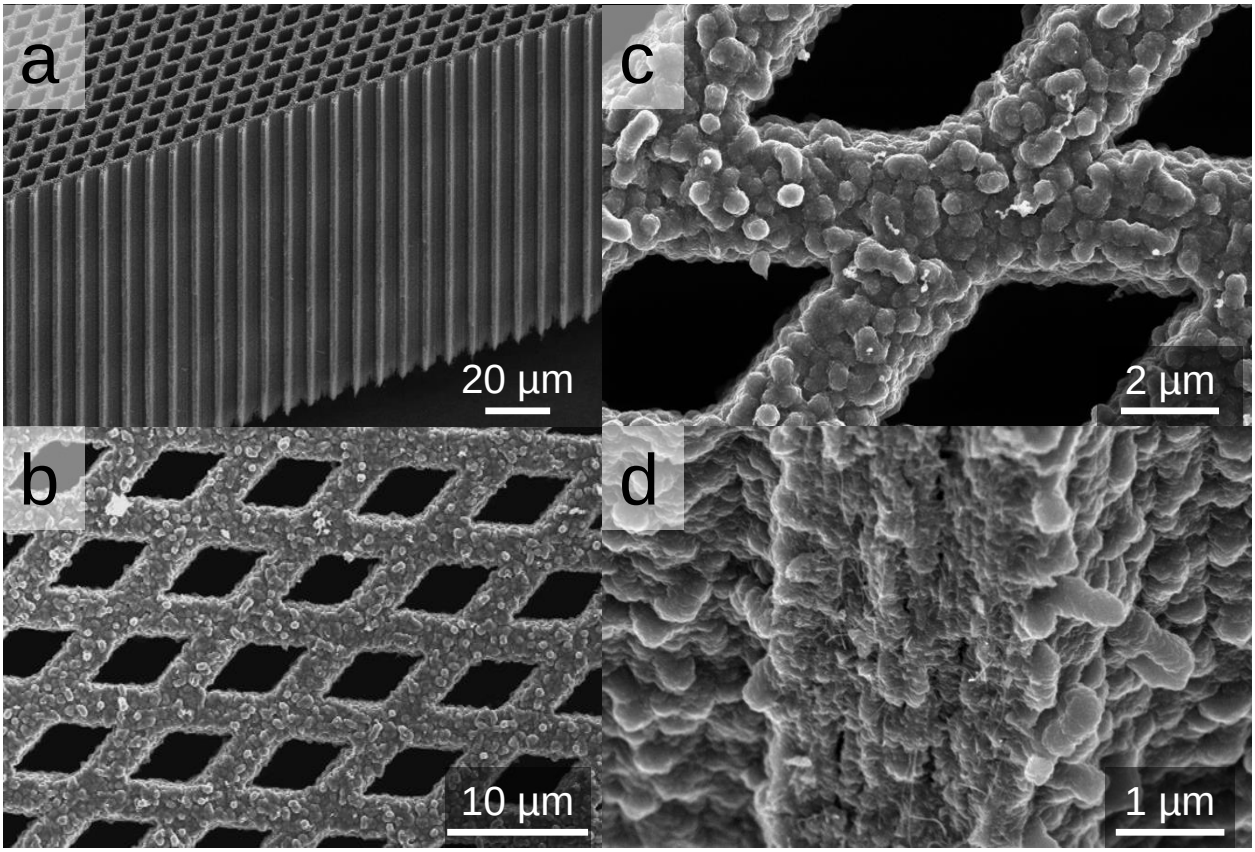


Figure 3.1 SEM images of 150 micron thick microsieve with 5 micron x 10 micron diamond shaped pores. a) Diamond pattern is visible on the top of structure. Vertical lines are a cross sectional view where the microsieve was broken. Shows uniformity and vertically of the channels. b) Top view of microsieve shows that lithographic diamond pattern is faithfully reproduced in the final three dimensional structure. c) High magnification view of microsieve top. Sidewall and surface roughness is much less than 1 micron. d) Cross sectional view where microsieve was broken. Center line is broken area showing that infiltration yielded a substantially solid structure.

3.1.2 Ultrahigh Surface Area Filter Characterization

Ultrahigh surface area filters with pores on the 50-100 nm range were fabricated. As shown in Figure 3.2, the 5 micron and 10 micron sidewalls were unstable in the geometry we used, but the thicker sidewalls (20 micron and 40 micron) grew cleanly (See Figure 3.2).

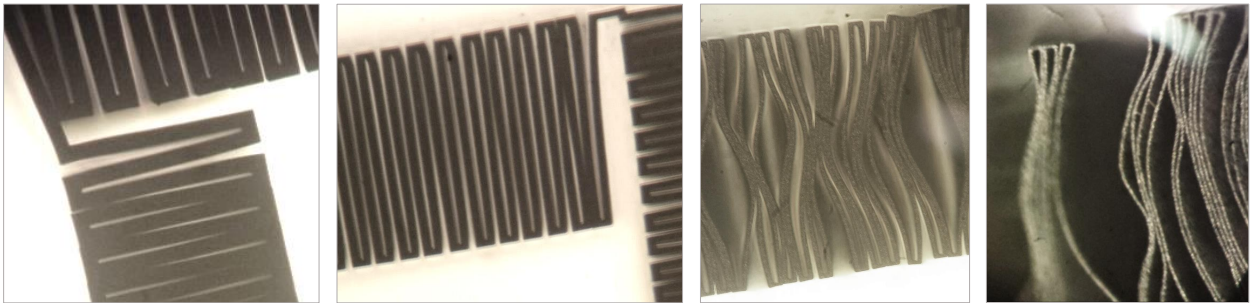


Figure 3.2 Ultrahigh Surface Area Filter Optical Images. Starting from the left the sidewall thicknesses are 40 micron, 20 micron, 10 micron, 5 micron.

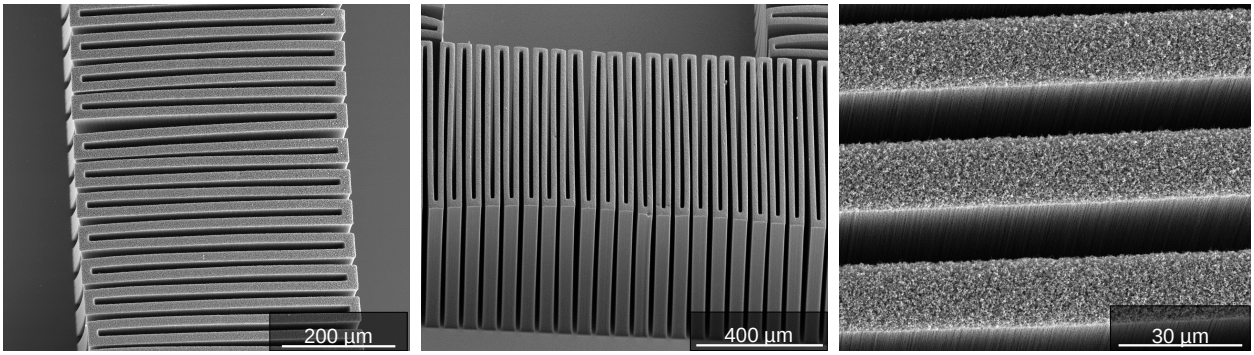


Figure 3.3 Ultrahigh Surface Area Filter SEM Images. Taken from a sample with 20 micron thick sidewalls.

3.2 Pressure vs Flow Rate Results

3.2.1 Microsive Flow Rate Results

Filter areas of 1.27 cm^2 showed flow rates around 105 mL/min at 2 PSI. See Figure 3.4. We compared these flow rates with those of commercial track etch membranes (a commonly used filter for applications requiring uniform pores) for which there is only data available at 10 PSI. In order to compare we extrapolated our data to estimate approximate flow rates at 10 PSI. This gives a good approximation because flow rates in this regime are highly linear with pressure. Using a linear fit of our data, we calculate a flow rate of approximately 400 mL/min/cm^2. 10-20 micron thick track etch membranes report flow rates of 700-800 mL/min/cm^2. See [9] and [10].

In a direct comparison these track etch membranes have significantly higher flow rates, but they are also much thinner (10-20 microns vs approximately 150 microns). Our process could be adjusted to make thinner filter membranes but they would be significantly weaker than the 150 micron version. The theoretical flow rate through circular orifices scales as 1/length [1]. If we use this to again extrapolate our data to a membrane that is the same thickness as the track etch membranes then we get flow rates that are approximately 5 times greater than that of the track etch membranes. More testing is required to confirm these predictions.

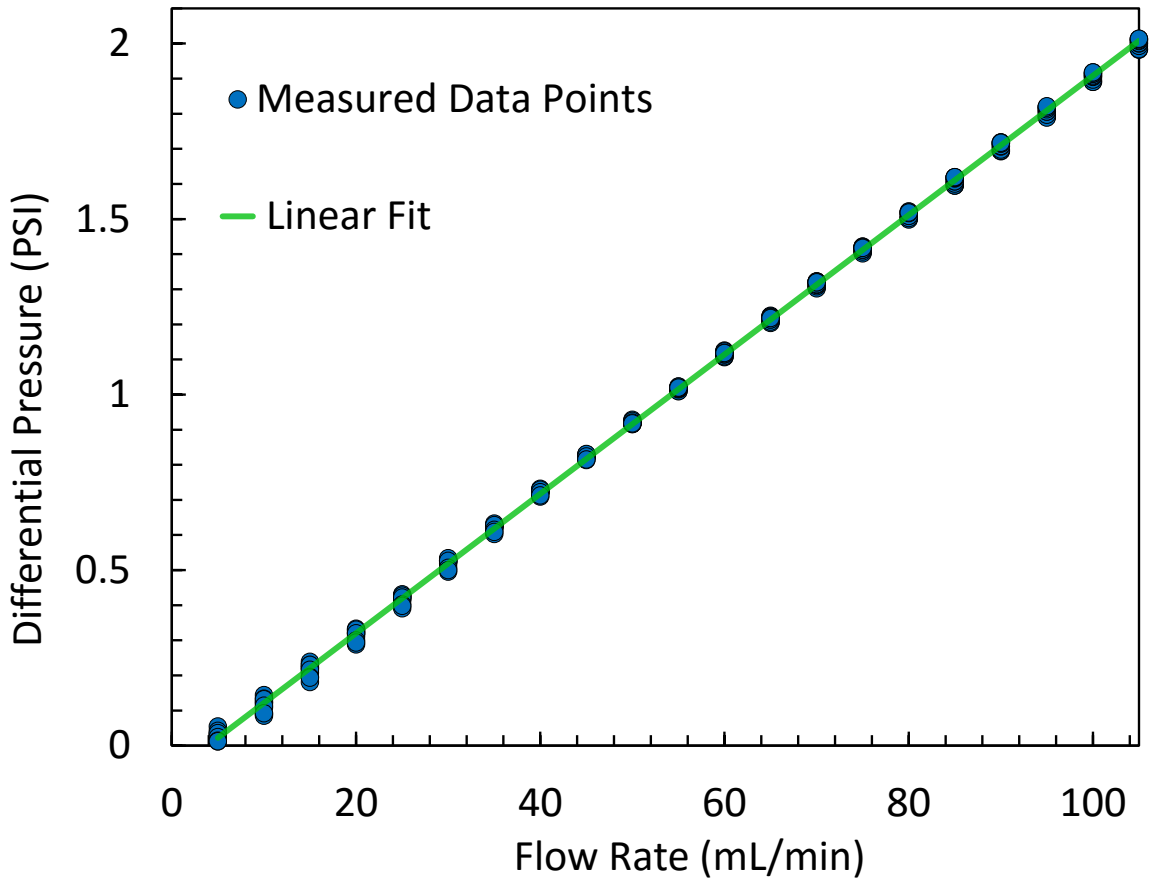


Figure 3.4 Flow Rate vs Pressure Testing on filter with a 1.27 cm^2 filter area. The flow rate was set at 5 mL/min increments from 5 mL/min to 105 mL/min and the pressure was measured at each flow rate was measured. This entire cycle was run ten times on the same filter to check for degradation in filter performance. All ten runs are plotted and no significant change was seen over the course of the ten runs. The fact that the plot does not show a 0 mL/min flow rate at 0 PSI (it doesn't go through the origin) indicates that our pressure calibration was off, showing slightly higher flow rates than the actual values. The trendline is y = 0.0199x - 0.077.

3.2.2 Ultrahigh Surface Area Filter Flow Results

Flow testing was performed on the ultrahigh surface area geometries in the same way as for the standard geometry. See Figure 3.5. The flow rates were then compared with published data on Millipore mixed cellulose ester filters with similar pore sizes [11]. See Table 3.1

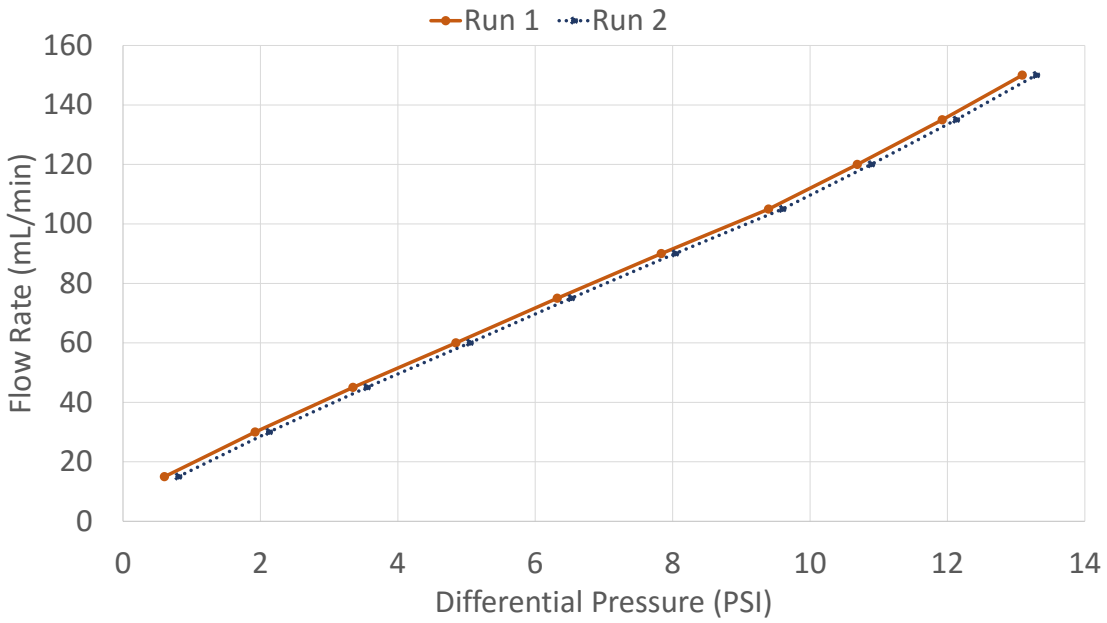


Figure 3.5 Ultrahigh Surface Area Filter Flow Rate Data

Table 3.1 Flow rate per filter area comparison of ultrahigh surface area Micropleated CNT-M filter vs standard Millipore mixed cellulose ester (MCE) disk filters [11]. All data is taken at 10 PSI.

Filter (Pore Size)	Flow Rate ($mL/min/cm^2$)
Micropleated CNT-M filter (50-100 nm)	275
Millipore MCE (50 nm)	0.75
Millipore MCE (100 nm)	1.5
Millipore MCE (200 nm)	18

3.3 Microsieve Efficiency Results

Filter efficiency testing was done using solutions of six micron and two micron fluorescent particles. With five micron pores, we expect the six micron particles to be blocked and the 2 micron particles to pass though. Two runs were performed with each particle size. By comparing fluorescence measurements of the post filtration solution and solutions of known relative concentrations a percent particle removal was obtained. The six micron particles showed there was no detectable fluorescence beyond that of deionized water indicating a filtration efficiency of at least 99.5%. See Figure 3.6 and 3.7. The two micron particles showed removal efficiencies of 33% and 6%. See Figure 3.8.

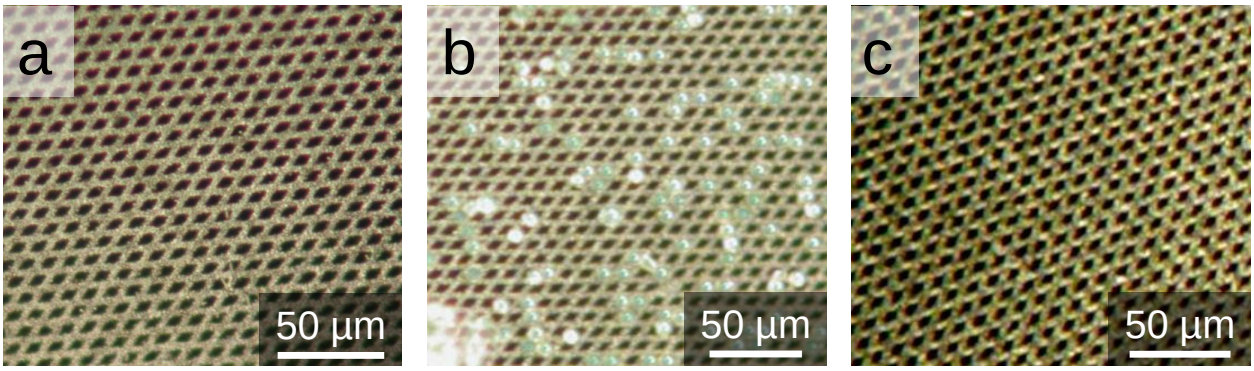


Figure 3.6 Optical microscope images of top of microsieve before and after efficiency testing. a) Filter is clean before filtration. b) Spheres are visible on the surface of the microsieve after filtration of 6 micron polystyrene bead solution. c) No spheres are visible after filtration of 2 micron polystyrene bead solution.

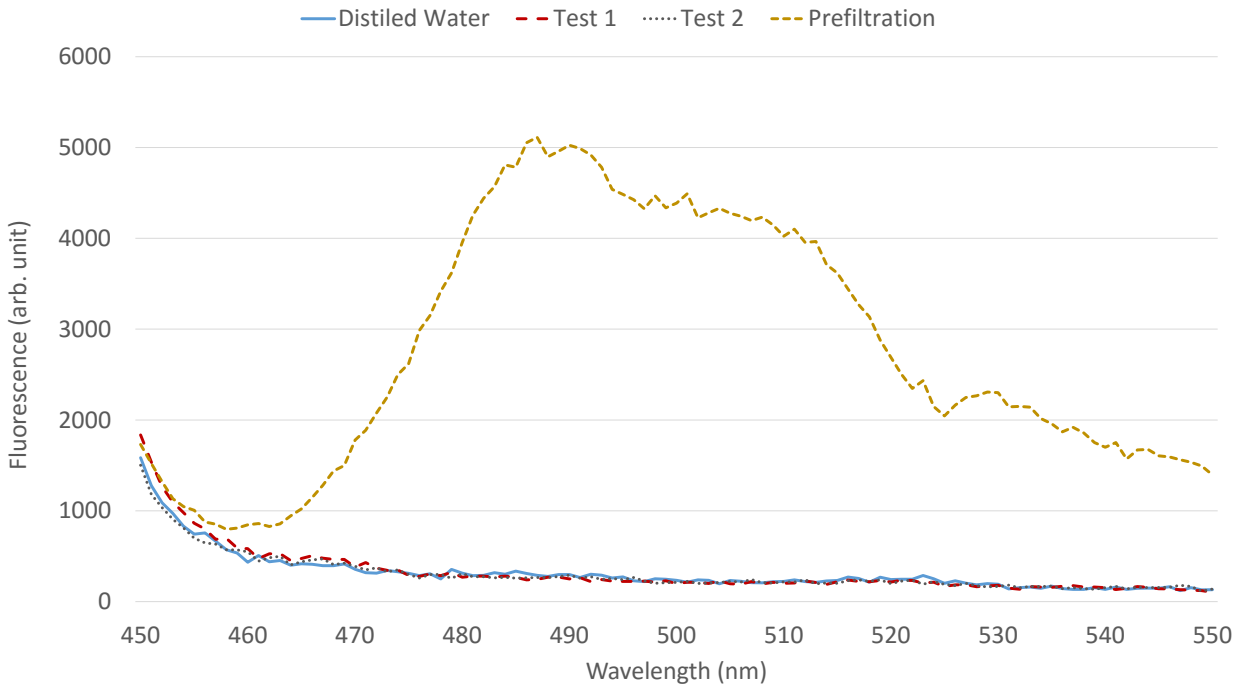


Figure 3.7 Fluorimetry for filter efficiency on 6 micron microspheres

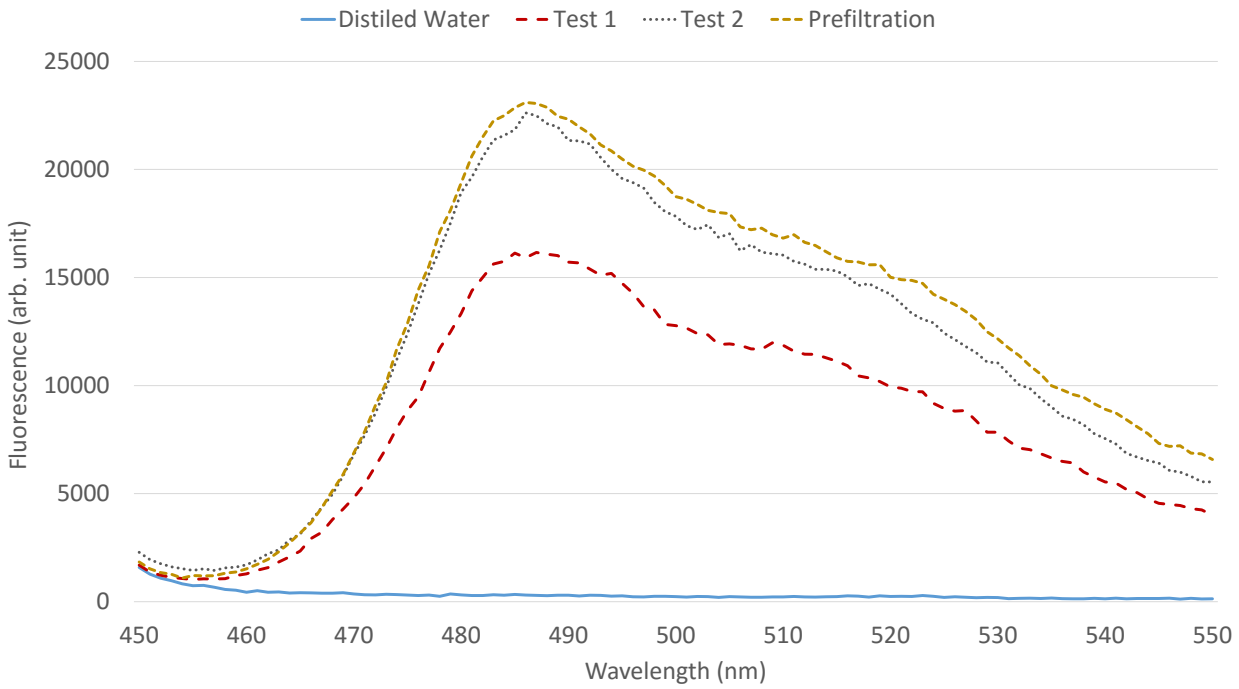


Figure 3.8 Fluorimetry for filter efficiency on 2 micron microspheres

3.4 Conclusion

We fabricated two types of fluid filters developed using carbon-nanotube-templated microfabrication (CNT-M). The first of these are high strength microsieves for both liquid and gas filtration. The sieves were fabricated by growing patterned forests of vertically aligned carbon nanotubes followed by an infiltration of the forest with nanocrystalline carbon. The process is compatible with the fabrication of sieves with pore sizes from below one micron up to tens of microns. Straight, vertical channels result in low flow resistance and the high strength carbon material is compatible with high pressure filtering. Initial filtration testing on sample sieves with 5 micron pores showed greater than 99.5% removal efficiencies of 6 micron particles. The second filter type also uses an adaptation of CNT-M to make high throughput filters by hierachically patterning the structure to achieve ultrahigh surface areas. These filters have pores on the order of 50-100 nm and therefore are compatible with bacterial filtration. Preliminary flow testing has shown flow rates of over 180 times greater than standard Millipore mixed cellulose ester sterilizing disk filters.

A patent application has been filed for the CNT-M microsieve [12]. A provisional patent has been submitted on the ultrahigh surface area filters.

Bibliography

[1] C. J. M. van Rijn, *Nano and micro engineered membrane technology*, 1st ed. ed. (Elsevier, Amsterdam; Boston, 2004).

[2] G. M. L. W. l. Coumans, Frank A. W.1van Dalum, "Filter Characteristics Influencing Circulating Tumor Cell Enrichment from Whole Blood.,", 2013.

[3] P.-V. L. J. G. R. M. Bikel, M.ÃĞulfaz, "Polymeric microsieves via phase separation microfabrication: Process and design optimization,", 2010.

[4] I. a. W. b. R. C. b. H. c. R. a. â. M. GironÃĺs, M. aAkbarsyah, "Polymeric microsieves produced by phase separation micromolding,", 2006.

[5] S. Kuiper, C. van Rijn, W. Nijdam, and M. Elwenspoek, "Development and applications of very high flux microfiltration membranes," Journal of Membrane Science **150,** 1–8 (1998), pT: J; UT: WOS:000076961600001.

[6] D. N. Hutchison, N. B. Morrill, Q. Aten, B. W. Turner, B. D. Jensen, L. L. Howell, R. R. Vanfleet, and R. C. Davis, "Carbon Nanotubes as a Framework for High-Aspect-Ratio MEMS Fabrication," Journal of Microelectromechanical Systems **19,** 75–82 (2010), pT: J; TC: 26; UT: WOS:000274213700008.

[7] J. Song, D. S. Jensen, D. N. Hutchison, B. Turner, T. Wood, A. Dadson, M. A. Vail, M. R. Linford, R. R. Vanfleet, and R. C. Davis, "Carbon-Nanotube-Templated Microfabrication of Porous Silicon-Carbon Materials with Application to Chemical Separations," Advanced Functional Materials **21,** 1132–1139 (2011), pT: J; UT: WOS:000288559100015.

[8] L. K. Barrett, D. J. Barton, S. G. Noyce, D. D. Allred, R. R. Vanfleet, and R. C. Davis, "High-Aspect-Ratio Metal Microfabrication by Nickel Electroplating of Patterned Carbon Nanotube Forests," Journal of Microelectromechanical Systems **24,** 1331–1337 (2015), iD: 1.

[9] "Content Tab, PCTE Membrane Filter Specifications,", 2016, [Online] Available from: http://www.sterlitech.com/filters/membrane-disc-filters/polycarbonate-membranes/hydrophilic-polycarbonate-membrane-filters/hydrophilic-polycarbonate-membrane-filter-pctb5047100.html. (Accessed: 2 April 2016).

[10] "Porosity and Typical Parameters of Track-Etched Membranes,", [Online] Available from: http://arb-ls.com/products/it4ip/porosity_and_typical_parameters.pdf. (Accessed: 2 April 2016).

[11] "Millidisk Cartridges and Millipak Disposable Capsules,", 2015, [Online] Available from: http://www.emdmillipore.com/Web-US-Site/en_CA/-/USD/ShowDocument-File?ProductSKU=MM_NF-C85052&DocumentId=201306.10805.ProNet&DocumentType=DS. (Accessed: 2 April 2016).

[12] A. Davis, R. Davis, and R. Vanfleet, "Microsieve using carbon nanotubes,", 2013, US Patent App. 13/624,083.

Index

carbon nanotube, 5, 7
Carbon Nanotube Templated Microfabrication, 2, 4, 5, 15
carbon nanotubes, 3
chemical vapor deposition, 7
CNT sidewall, 9

flow rate, 1, 3, 12, 13, 18–20

infiltration, 3, 5, 7, 16

microsieves, 1

particle removal efficiency, 3, 14, 21, 22
photolithography, 6

scanning electron microscope, 16, 17

ultrahigh surface area, 8, 10–13, 17, 20